10^{th} International Conference on Fracture Mechanics of Concrete and Concrete Structures
FraMCoS-X
G. Pijaudier-Cabot, P. Grassl and C. La Borderie (Eds)
https://doi.org/10.21012/FC10.233196

MICROPLANE DAMAGE PLASTIC MODEL FOR PLAIN CONCRETE SUBJECTED TO COMPRESSIVE FATIGUE LOADING

A. BAKTHEER*, M. AGUILAR*, J. HEGGER* and R. CHUDOBA*

*Institute of Structural Concrete, RWTH Aachen University
Mies-van-der-Rohe-Straße 1 , 52074 Aachen , Germany
E-mail: Abaktheer@imb.rwth-aachen.de

Key words: Concrete fatigue, Microplane theory, Fatigue damage, Thermodynamics

Abstract. A thermodynamically based microplane fatigue damage model for plain concrete under compressive loading is introduced. The key idea of the present approach is to relate the fatigue damage to a cumulative measure of inelastic sliding/shear strains. Which reflects the fatigue damage accumulation owing to internal friction at subcritical fatigue loading level. The model is formulated within the microplane framework using a homogenization approach based on the energy equivalence principle with explicit representation of the effective triaxial elastic stiffness. The model can reflect the damage-induced anisotropic behavior of concrete and can reproduce the shape of the hysteretic loops related to the fatigue damage development within the tensorial representation of the material state. Elementary studies of the model response and its applicability to modeling of the fatigue response under compression are presented. The ability to reproduce the typical shape of the hysteretic loops is discussed and compared to the existing phenomenological fatigue models for concrete under compression.

1 INTRODUCTION

The paramount requirement for economic and reliable design of concrete structures subjected to cyclic loading is a profound characterization of resistance to fatigue loading. Relevant examples of structures which have to resist up to 10 millions of loading cycles are road and railway bridges, as well as onshore and offshore wind turbine towers. A deeper insight into the fatigue behavior is needed to significantly reduce the material consumption, to enhance the service life and to increase the reliability of engineering structures.

Characterization of concrete fatigue behavior is a challenging task that has increasingly attracted attention of researchers during the past decades. Besides extensive experimental investigations, several attempts have been made to develop reliable numerical models. However, while for metals underlying microstructural mechanisms governing the fatigue damage propagation are well known, the fatigue damage phenomenology of concrete is still not sufficiently understood. Therefore, advanced numerical models for concrete fatigue are needed to comprehensively describe and interpret the fundamental mechanisms governing the fatigue damage evolution and propagation.

Numerical models of fatigue damage propagation in concrete can be classified into two groups. In the first group the concrete fatigue behavior is described as a function of performed loading cycles, whereas the second group of models is based on the damage mechanics theory with the fatigue damage related to a measure of strain. The discussed types of models are summarized in Table. 1. Several analytical and empirical equations have been devel-

Table 1: General classification of approaches to modeling of concrete fatigue

Lifetime based approaches		**Strain based approaches**		
Strain approximations	Damage approximations	Tensorial models	Microplane models	Discrete models
Liu [1]	Pfanner [2]	Alliche [4] Desmorat [6]	Kirane and Bazant [8]	Wang [9]

oped in the last decades describing the fatigue behavior of concrete on the lifetime scale [1]. In this class of models the strain evolution during fatigue life i.e. fatigue creep curves are reproduced based on experimental observations. Pragmatic approaches to fatigue damage modeling use the number of performed loading cycles directly as a damage driving state variable [2]. More advanced approaches to simulation of fatigue damage process cycle by cycle at subcritical load levels have been proposed in the literature with damage related either to total strain [3,4], or to the inelastic strain [5]. In order to reflect the opening/closure and growth of microcracks and/or the frictional sliding along their lips, the formulation of the dissipative mechanisms has been refined by introducing the internal sliding strain as a fatigue damage driving variable [6]. An approach relating the dissipative terms owing to fatigue damage even closer to the observable disintegration mechanisms within the material structure appeared recently in [8]. The key idea of this model is to relate the damage evolution to the cumulative measure of volumetric strain. Further discrete lattice models have been developed recently e.g. [9].

Microplane model formulation can be regarded as a coupled multiscale model. Indeed, it introduces an additional level of state representation below the level of material point. Even though this level does not have the ambition to reflect the spatial layout of the material microstructure, it can reflect a damage pattern and its anisotropic evolution during the loading in a smeared way. It applies the concept of kinematic constraint and stress homogenization in order to establish a link between the macroscopic and microplane level of discretization [10].

Fatigue damage developing at subcritical load levels includes several interacting mechanisms: development and coalescence of microcracks, repeated crack opening and closure, internal sliding and friction. The roughness of cracked surfaces and the interlocking of aggregates generates inelastic strain and induces frictional sliding within the microcrack network. Thus, the crucial aspect of fatigue modeling is the representation of inelastic dissipation owing to damage, i.e. the development of microcracks, and internal frictional sliding at the edges of the inherent material discontinuities within the deteriorating structure. The aim of the present paper is the represent the described fatigue damage propagation mechanisms within a numerical phenomenological material models of microplane type. The resolution of the stress and strain states at the level of microplane provided the possibility to reflect the microscopic interaction of normal and pressure sensitive friction dissipative mechanisms see Fig 1.

In this paper we introduce a thermodynamically consistent microplane fatigue damage model for plain concrete. The key idea of this model is to relate the fatigue damage to a cumulative measure of inelastic sliding/shear strains. Which reflects the fatigue damage accumulation owing to internal friction at subcritical loading levels.

2 MICROPLANE FATIGUE MODEL

Unlike the classical constitutive models with a direct relation between the strain and stress tensors, the microplane models introduces the constitutive relation between strain and stress vectors at the level of planes projected to a unit hemisphere centered at a material point. The

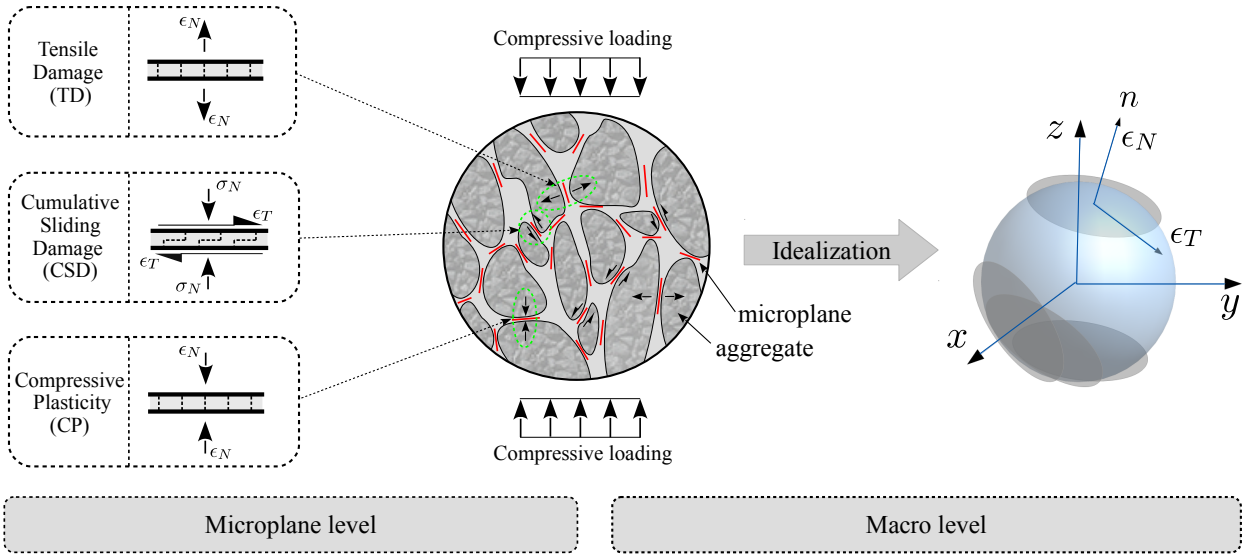

Figure 1: Dissipative mechanisms of the proposed microplane model: illustration of the idealized microstructure with system of assumed microplanes and the load transfer mechanisms under compression loading

mapping from the strain tensor to the stress tensor is done in several steps, starting with a projection onto the oriented microplanes that can be viewed as a discretization of the tensor state. In the second step, the constitutive law is evaluated at each microplane to obtain the stress vector. Finally, the stress tensor is obtained by numerically integrating the stress contributions over the whole hemisphere, i.e. all microplanes.

2.1 Kinematic constraint

The strain tensor is projected onto the microplane to obtain strain vectors consisting of the normal and tangential components using the so called kinematic constraint

$$\varepsilon_{\mathrm{N}} = \boldsymbol{N} : \boldsymbol{\varepsilon}, \qquad \boldsymbol{\varepsilon}_{\mathbf{T}} = \mathbf{T} : \boldsymbol{\varepsilon}, \tag{1}$$

where the scalar ε_{N} is the normal microplane strain, and $\boldsymbol{\varepsilon}_{\mathbf{T}}$ is the tangential microplane strain vector. The second order normal tensor $\boldsymbol{N}$ and the third order tangential tensor $\boldsymbol{T}$ are given as

$$\boldsymbol{N} = \boldsymbol{n} \otimes \boldsymbol{n}, \tag{2}$$

$$\mathbf{T} = \boldsymbol{n} \cdot \mathbb{I}_{sym} - \boldsymbol{n} \otimes \boldsymbol{n} \otimes \boldsymbol{n}, \tag{3}$$

where $\boldsymbol{n}$ is the microplane normal vector and $\mathbb{I}$ is the fourth-order identity tensor.

2.2 Microplane constitutive laws

Normal direction: Thermodynamically based constitutive laws governing the macroscopic behavior are defined on the generic microplanes by introducing the dissipative mechanisms that are illustrated in Fig. 1. The macroscopic thermodynamic potential is expressed as the sum of normal and tangential Helmholtz free energies

$$\begin{aligned}\psi^{\mathrm{mac}} &= \frac{3}{2\pi}\int_{\Omega}\psi^{\mathrm{mic}}d\Omega \\ &= \frac{3}{2\pi}\int_{\Omega}\psi_{\mathrm{N}}^{\mathrm{mic}}d\Omega + \frac{3}{2\pi}\int_{\Omega}\psi_{\mathrm{T}}^{\mathrm{mic}}d\Omega \end{aligned} \tag{4}$$

The microplane thermodynamic potential of the normal direction is expressed as

$$\begin{aligned}\rho\psi_{\mathrm{N}}^{\mathrm{mic}} &= \frac{1}{2}\left[1 - H(\sigma_{\mathrm{N}})\,\omega_{\mathrm{N}}\right] E_{\mathrm{N}}(\varepsilon_{\mathrm{N}} - \varepsilon_{\mathrm{N}}^{\mathrm{p}})^2 \\ &\quad + \frac{1}{2}K_{\mathrm{N}}z_{\mathrm{N}}^2 + \frac{1}{2}\gamma_{\mathrm{N}}\alpha_{\mathrm{N}}^2 + f(r_{\mathrm{N}}),\end{aligned} \tag{5}$$

with $\psi_{\mathrm{N}}^{\mathrm{mic}}$ denoting the Helmholtz free energy of the normal direction, ρ the material density and $E_{\mathrm{N}} = E/(1-2\nu)$ the normal elastic stiffness which is defined as a function of the Young's modulus E and the Poisson's ratio ν. $H(\sigma_{\mathrm{N}})$ is a Heaviside function for switching the normal behavior, i. e. damage under tension $H(\sigma_{\mathrm{N}}^{+}) = 1$, and plasticity under compression $H(\sigma_{\mathrm{N}}^{-}) = 0$, K_{N} and γ_{N} are the isotropic

and kinematic hardening moduli, respectively. The thermodynamic internal variables are plastic normal strain $\varepsilon_{\mathrm{N}}^{\mathrm{p}}$ defining the irreversible strain, damage variable ω_{N} ranging from 0 to 1, the internal variables of isotropic hardening z_{N} and kinematic hardening α_{N}. The function $f(r_{\mathrm{N}})$ defines a consolidation function associated with damage. The thermodynamic forces are obtained by differentiating the thermodynamic potential (5) with respect to each internal variable. Therefore, the normal stress is obtained as

$$\sigma_{\mathrm{N}} = \frac{\partial \rho \psi_{\mathrm{N}}}{\partial \varepsilon_{\mathrm{N}}} = \left[1 - H(\sigma_{\mathrm{N}})\, \omega_{\mathrm{N}}\right] E_{\mathrm{N}} (\varepsilon_{\mathrm{N}} - \varepsilon_{\mathrm{N}}^{\mathrm{P}}). \tag{6}$$

The thermodynamic hardening forces can be obtained as

$$Z_{\mathrm{N}} = \frac{\partial \rho \psi_{\mathrm{N}}}{\partial z_{\mathrm{N}}} = K_{\mathrm{N}} z_{\mathrm{N}}, \tag{7}$$

$$X_{\mathrm{N}} = \frac{\partial \rho \psi_{\mathrm{N}}}{\partial \alpha_{\mathrm{N}}} = \gamma_{\mathrm{N}} \alpha_{\mathrm{N}}, \tag{8}$$

the energy release rate related to damage state variable reads

$$Y_{\mathrm{N}} = \frac{\partial \rho \psi_{\mathrm{N}}}{\partial \omega_{\mathrm{N}}} = \frac{1}{2} H(\sigma_{\mathrm{N}}) E_{\mathrm{N}} (\varepsilon_{\mathrm{N}} - \varepsilon_{\mathrm{N}}^{\mathrm{p}})^2. \tag{9}$$

Similarly to [12], the thermodynamic force associated with the damage consolidation is defined as

$$R_{\mathrm{N}} = \frac{\partial \rho \psi_{\mathrm{N}}}{\partial r_{\mathrm{N}}} = \frac{1}{A_{\mathrm{d}}} \left[\frac{-r_{\mathrm{N}}}{1 + r_{\mathrm{N}}} \right]. \tag{10}$$

where A_{d} is a material parameter defining the brittleness of the damage evolution. The yield function of the plasticity governed compressive behavior, delimited with the help of the Heaviside step function $H(.)$, is expressed as

$$f_{\mathrm{N}}^{\mathrm{p}} = H(-\sigma_{\mathrm{N}}) |\tilde{\sigma}_{\mathrm{N}} - X_{\mathrm{N}}| - (Z_{\mathrm{N}} + \sigma_{\mathrm{N}}^{0}) \leq 0, \tag{11}$$

where σ_{N}^{0} is the plastic yielding stress. The flow potential is extended by a non-associative term introducing a nonlinear hardening as

$$\phi_{\mathrm{N}}^{\mathrm{p}} = f_{\mathrm{N}}^{\mathrm{p}} + \frac{1}{2} m X_{\mathrm{N}}^{2}, \tag{12}$$

where m is the nonlinear hardening parameter. The threshold function governing the damage evolution is defined as

$$f_{\mathrm{N}}^{\omega} = Y_{\mathrm{N}} - (Y_{\mathrm{N}}^{0} + R_{\mathrm{N}}) \leq 0, \tag{13}$$

where the energy release rate threshold is $Y_{\mathrm{N}}^{0} = \frac{1}{2} E_{\mathrm{N}} (\varepsilon_{\mathrm{N}}^{0})^2$ and $\varepsilon_{\mathrm{N}}^{0}$ is the elastic threshold normal strain. The evolution laws are obtained by differentiating the flow potential for plasticity (12) and the damage threshold function (13) with respect to the thermodynamic forces

$$\dot{\varepsilon}_{\mathrm{N}}^{\mathrm{p}} = \dot{\lambda}_{\mathrm{N}}^{\mathrm{p}} \frac{\partial f_{\mathrm{N}}^{\mathrm{p}}}{\partial \sigma_{\mathrm{N}}} = \dot{\lambda}_{\mathrm{N}}^{\mathrm{p}}\, \mathrm{sign}(\sigma_{\mathrm{N}} - X_{\mathrm{N}}) \tag{14}$$

$$\dot{z}_{\mathrm{N}} = -\dot{\lambda}_{\mathrm{N}}^{\mathrm{p}} \frac{\partial f_{\mathrm{N}}^{\mathrm{p}}}{\partial Z_{\mathrm{N}}} = \dot{\lambda}_{\mathrm{N}}^{\mathrm{p}} \tag{15}$$

$$\dot{\alpha_{\mathrm{N}}} = -\dot{\lambda}_{\mathrm{N}}^{\mathrm{p}} \frac{\partial f_{\mathrm{N}}^{\mathrm{p}}}{\partial X_{\mathrm{N}}} = \dot{\lambda}_{\mathrm{N}}^{\mathrm{p}} \left[\mathrm{sign}(\sigma_{\mathrm{N}} - X_{\mathrm{N}}) + m\, X_{\mathrm{N}}\right] \tag{16}$$

$$\dot{\omega}_{\mathrm{N}} = \dot{\lambda}_{\mathrm{N}}^{\omega} \frac{\partial f_{\mathrm{N}}^{\omega}}{\partial Y_{\mathrm{N}}} = \dot{\lambda}_{\mathrm{N}}^{\omega} \tag{17}$$

$$\dot{r}_{\mathrm{N}} = -\dot{\lambda}_{\mathrm{N}}^{\omega} \frac{\partial f_{\mathrm{N}}^{\omega}}{\partial R_{\mathrm{N}}} = -\dot{\lambda}_{\mathrm{N}}^{\omega}. \tag{18}$$

The consistency condition for the plastic yield function reads

$$\dot{f}_{\mathrm{N}}^{\mathrm{p}} = \dot{\sigma}_{\mathrm{N}} \frac{\partial f_{\mathrm{N}}^{\mathrm{P}}}{\partial \sigma_{\mathrm{N}}} + \dot{X}_{\mathrm{N}} \frac{\partial f_{\mathrm{N}}^{\mathrm{p}}}{\partial X_{\mathrm{N}}} + \dot{Z}_{\mathrm{N}} \frac{\partial f_{\mathrm{N}}^{\mathrm{p}}}{\partial Z_{\mathrm{N}}} = 0. \tag{19}$$

By substituting the evolution equations (14-16) into the consistency condition the plastic multiplier can be obtained

$$\dot{\lambda}_{\mathrm{N}}^{\mathrm{p}} = \frac{E_{\mathrm{N}}\, \dot{\varepsilon}_{\mathrm{N}}\, \mathrm{sign}(\sigma_{\mathrm{N}} - X_{\mathrm{N}})}{E_{\mathrm{N}} + K_{\mathrm{N}} + \gamma_{\mathrm{N}} \left[1 + m\, X_{\mathrm{N}}\, \mathrm{sign}(\sigma_{\mathrm{N}} - X_{\mathrm{N}})\right]}. \tag{20}$$

In a similar way, the damage multiplier is obtained using equations (17-18) as

$$\dot{\lambda}_{\mathrm{N}}^{\omega} = 1 - \frac{1}{1 + A_{\mathrm{d}} (Y_{\mathrm{N}} - Y_{0})}. \tag{21}$$

Energy dissipation associated with the normal inelastic mechanisms can be given as

$$\mathcal{D}_{\mathrm{N}}^{\mathrm{mic}} = \sigma_{\mathrm{N}}\, \dot{\varepsilon}_{\mathrm{N}}^{\mathrm{p}} - X_{\mathrm{N}}\, \dot{\alpha_{\mathrm{N}}} - K_{\mathrm{N}}\, \dot{z}_{\mathrm{N}} + Y_{\mathrm{N}}\, \dot{\omega}_{\mathrm{N}}. \tag{22}$$

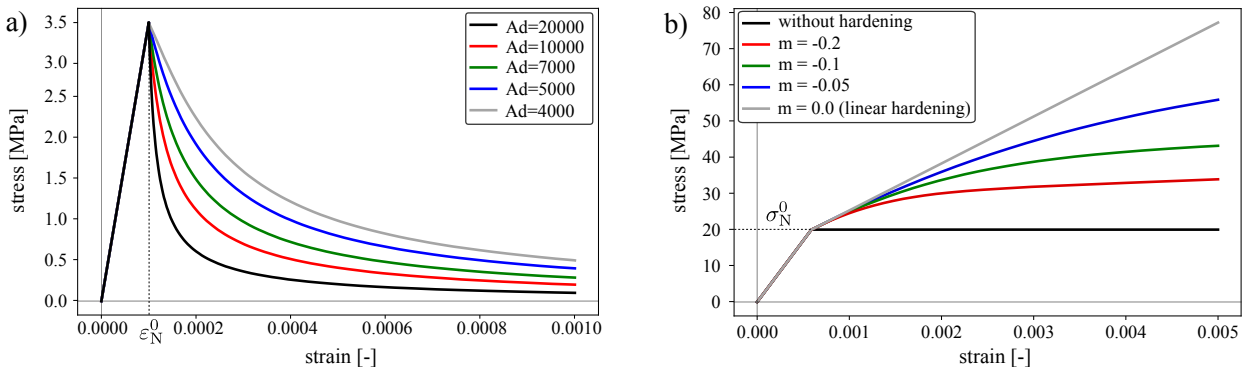

Figure 2: The uniaxial normal behavior at the microplane level: a) tensile damage (TD) for different values of the brittleness parameter A_{d}; b) compressive plasticity (CP) for different hardening cases

The illustration of the uniaxial normal behavior at the microplane level is presented in Fig. 2. The tensile behavior governed by the damage is depicted in Fig. 2a, for different values of the brittleness parameter A_{d}. On the other hand, the plastic behavior under compression is shown in Fig. 2b, for different cases of hardening.

Tangential direction: To introduce a mechanism driving the material deterioration at subcritical load levels we assume that the tangential cumulative damage is the fundamental source of fatigue damage. The tangential behavior of a microplane is described using the pressure sensitive interface model with fatigue damage driven by cumulative inelastic slip presented in [13]. In this model the thermodynamic potential for the tangential state variables is given as

$$\rho\psi_{\mathrm{T}}^{\mathrm{mic}} = \frac{1}{2}(1-\omega_{\mathrm{T}})E_{\mathrm{T}}(\boldsymbol{\varepsilon_{\mathrm{T}}}-\boldsymbol{\varepsilon_{\mathrm{T}}^{\pi}})\cdot(\boldsymbol{\varepsilon_{\mathrm{T}}}-\boldsymbol{\varepsilon_{\mathrm{T}}^{\pi}}) + \frac{1}{2}K_{\mathrm{T}}z_{\mathrm{T}}^{2} + \frac{1}{2}\gamma_{\mathrm{T}}\boldsymbol{\alpha_{\mathrm{T}}}\cdot\boldsymbol{\alpha_{\mathrm{T}}} \tag{23}$$

where $\psi_{\mathrm{T}}^{\mathrm{mic}}$ is the Helmholtz free energy of the tangential direction, the tangential elastic stiffness is E_{T}, K_{T} and γ_{T} are the isotropic and kinematic hardening moduli, respectively. The thermodynamic internal variables are the inelastic tangential strain vector, i.e. the sliding strain vector defining the irreversible strain $\varepsilon_{\mathrm{T}}^{\pi}$, the damage variable ω_{T} ranging from 0 to 1, the internal variables of isotropic hardening z_{T} and kinematic hardening vector $\boldsymbol{\alpha_{\mathrm{T}}}$. The corresponding thermodynamic forces are obtained by differentiating the thermodynamic potential (23) with respect to each internal variable, i. e.

$$\boldsymbol{\sigma_{\mathrm{T}}} = \frac{\partial\rho\psi_{\mathrm{T}}}{\partial\boldsymbol{\varepsilon_{\mathrm{T}}}} = (1-\omega_{\mathrm{T}})E_{\mathrm{T}}(\boldsymbol{\varepsilon_{\mathrm{T}}}-\boldsymbol{\varepsilon_{\mathrm{T}}^{\pi}}) \tag{24}$$

$$\boldsymbol{\sigma_{\mathrm{T}}^{\pi}} = -\frac{\partial\rho\psi_{\mathrm{T}}}{\partial\boldsymbol{\varepsilon_{\mathrm{T}}^{\pi}}} = (1-\omega_{\mathrm{T}})E_{\mathrm{T}}(\boldsymbol{\varepsilon_{\mathrm{T}}}-\boldsymbol{\varepsilon_{\mathrm{T}}^{\pi}}) \tag{25}$$

$$\boldsymbol{X}_{\mathrm{T}} = \frac{\partial\rho\psi_{\mathrm{T}}}{\partial\boldsymbol{\alpha_{\mathrm{T}}}} = \gamma_{\mathrm{T}}\boldsymbol{\alpha_{\mathrm{T}}} \tag{26}$$

$$Z_{\mathrm{T}} = \frac{\partial\rho\psi_{\mathrm{T}}}{\partial z_{\mathrm{T}}} = K_{\mathrm{T}}z_{\mathrm{T}} \tag{27}$$

$$Y_{\mathrm{T}} = \frac{\partial\rho\psi_{\mathrm{T}}}{\partial\omega_{\mathrm{T}}} = \frac{1}{2}E_{\mathrm{T}}(\boldsymbol{\varepsilon_{\mathrm{T}}}-\boldsymbol{\varepsilon_{\mathrm{T}}^{\pi}})\cdot(\boldsymbol{\varepsilon_{\mathrm{T}}}-\boldsymbol{\varepsilon_{\mathrm{T}}^{\pi}}). \tag{28}$$

The effective sliding stress can be written as

$$\tilde{\boldsymbol{\sigma}}_{\mathbf{T}}^{\boldsymbol{\pi}} = \frac{\boldsymbol{\sigma_{\mathrm{T}}^{\pi}}}{1-\omega_{\mathrm{T}}} = E_{\mathrm{T}}(\boldsymbol{\varepsilon_{\mathrm{T}}}-\boldsymbol{\varepsilon_{\mathrm{T}}^{\pi}}). \tag{29}$$

The threshold function is defined similarly to plasticity theory and including the sensitivity to the lateral pressure

$$f_{\mathrm{T}} = ||\tilde{\boldsymbol{\sigma}}_{\mathbf{T}}^{\boldsymbol{\pi}} - \boldsymbol{X_{\mathrm{T}}}|| - Z - \sigma_{\mathrm{T}}^{0} + a\,\sigma_{N} \tag{30}$$

where $||.||$ represents the norm of the vector, σ_{T}^{0} the tangential reversibility limit, σ_N is the normal microplane stress, and a is the pressure sensitivity parameter. The non-associative flow potentials defined as

$$\phi_{\mathrm{T}} = f_{\mathrm{T}} + \frac{S(1-\omega_{\mathrm{T}})^{c}}{(r+1)}\left(\frac{\sigma_{\mathrm{T}}^{0}}{\sigma_{\mathrm{T}}^{0}-a\,\sigma_{N}}\right)\left(\frac{Y_{\mathrm{T}}}{S}\right)^{r+1} \tag{31}$$

This flow potential is a modified function of the Lemaitre's damage potential presented in [7]. By differentiating the flow potential with respect to the thermodynamic forces, the evolution equations for all state variables are obtained as

$$\dot{\boldsymbol{\varepsilon}}^{\boldsymbol{\pi}}_{\mathbf{T}} = \dot{\lambda}^{\pi}_{\mathrm{T}} \frac{\partial \phi_{\mathrm{T}}}{\partial \boldsymbol{\sigma}^{\boldsymbol{\pi}}_{\mathbf{T}}} = \frac{\dot{\lambda}^{\pi}_{\mathrm{T}}}{1-\omega_{\mathrm{T}}} \frac{\tilde{\boldsymbol{\sigma}}^{\boldsymbol{\pi}}_{\mathbf{T}} - \boldsymbol{X}_{\mathbf{T}}}{||\tilde{\boldsymbol{\sigma}}^{\boldsymbol{\pi}}_{\mathbf{T}} - \boldsymbol{X}_{\mathbf{T}}||} \tag{32}$$

$$\dot{z}_{\mathrm{T}} = -\dot{\lambda}^{\pi}_{\mathrm{T}} \frac{\partial \phi_{T}}{\partial Z_{\mathrm{T}}} = \dot{\lambda}^{\pi}_{\mathrm{T}} \tag{33}$$

$$\dot{\boldsymbol{\alpha}}_{\mathbf{T}} = -\dot{\lambda}^{\pi}_{\mathrm{T}} \frac{\partial \phi_{\mathrm{T}}}{\partial \boldsymbol{X}_{\mathbf{T}}} = \dot{\lambda}^{\pi}_{\mathrm{T}} \frac{\tilde{\boldsymbol{\sigma}}^{\boldsymbol{\pi}}_{\mathbf{T}} - \boldsymbol{X}}{||\tilde{\boldsymbol{\sigma}}^{\boldsymbol{\pi}}_{\mathbf{T}} - \boldsymbol{X}||} \tag{34}$$

$$\begin{aligned} \dot{\omega}_{\mathrm{T}} &= \dot{\lambda}^{\pi}_{\mathrm{T}} \frac{\partial \phi_{\mathrm{T}}}{\partial Y_{\mathrm{T}}} \\ &= (1-\omega_{\mathrm{T}})^{c} \left(\frac{\sigma^{0}_{\mathrm{T}}}{\sigma^{0}_{\mathrm{T}} - a\ \sigma_{N}} \right) \left(\frac{Y_{\mathrm{T}}}{S} \right)^{r} \dot{\lambda}^{\pi}_{\mathrm{T}}. \end{aligned} \tag{35}$$

In analogy to the normal direction, the consistency condition is used to resolve the sliding multiplier as

$$\dot{\lambda}^{\pi}_{\mathrm{T}} = \frac{E_{\mathrm{T}}\ \dot{\boldsymbol{\varepsilon}}_{\mathbf{T}} \cdot\ (\tilde{\boldsymbol{\sigma}}^{\boldsymbol{\pi}}_{\mathbf{T}} - \boldsymbol{X})/||\tilde{\boldsymbol{\sigma}}^{\boldsymbol{\pi}}_{\mathbf{T}} - \boldsymbol{X}||}{E_{\mathrm{T}}/(1-\omega_{\mathrm{T}}) + K_{\mathrm{T}} + \gamma_{\mathrm{T}}}. \tag{36}$$

Finally, the energy dissipation of the tangential dissipative mechanisms reads

$$\mathcal{D}^{\mathrm{mic}}_{\mathrm{T}} = \boldsymbol{\sigma}^{\boldsymbol{\pi}}_{\mathbf{T}} \cdot \dot{\boldsymbol{\varepsilon}}^{\boldsymbol{\pi}}_{\mathbf{T}} - \boldsymbol{X}_{\mathbf{T}} \cdot \dot{\boldsymbol{\alpha}}_{\mathbf{T}} - K_{\mathrm{T}}\ \dot{z}_{\mathrm{T}} + Y_{\mathrm{T}}\ \dot{\omega}_{\mathrm{T}}. \tag{37}$$

To illustrate the proposed cumulative sliding behavior of tangential microplane direction, an elementary example of the tangential stress - strain relationship under monotonic and cyclic strain controlled loading is depicted in Fig. 3a showing the degradation of the stress under cyclic loading. The corresponding evolution of the damage is shown in Fig. 3b. This behavior is essential for the model to include the fatigue damage owing to the internal frictional sliding.

The damage law used in the model (35) is based on a modified function of the Lemaitres damage potential [7]. The reason for this modification is the fact that the shape of the damage relation with the cumulative sliding strain resulting from the original Lemaitre's damage potential is approaching $\omega = 1.0$ in a non-asymptotic manner. As demonstrated by Kirane and Bažant [8] when linking the damage to a cumulative measure of strain with the goal to cover the high cycle fatigue behavior, damage must be accumulated slowly, within a large range of cumulative strain approaching $\omega = 1.0$ asymptotically. The behavior of the modified damage potential is studied in Fig. 4 for cyclic loading with an upper load level increasing until failure showing a slower evolution of damage along the cumulative sliding strain, asymptotically approaching the value $\omega = 1.0$.

2.3 Homogenization

The homogenization approach based on the principle of energy equivalence, exemplified e.g. in [11], is used for the damage in this study. This principle works with the effective stress and strain tensors $\tilde{\varepsilon}, \tilde{\boldsymbol{\sigma}}$. These effective quantities reflect the condition of the undamaged material and the relation between the effective strain and stress tensors can be written as follows

$$\tilde{\boldsymbol{\sigma}} = \boldsymbol{C}^{\mathrm{e}} : \tilde{\boldsymbol{\varepsilon}}, \tag{38}$$

where $\boldsymbol{C}^{\mathrm{e}}$ is the fourth order elastic stiffness tensor. The relation between the macroscopic stress tenser $\boldsymbol{\sigma}$ and the effective stress tensor $\tilde{\boldsymbol{\sigma}}$ is given as follows

$$\boldsymbol{\sigma} = \boldsymbol{\beta} : \tilde{\boldsymbol{\sigma}}, \tag{39}$$

where $\boldsymbol{\beta}$ is the fourth order damage inverse/integrity tensor. The relation between the effective strain tensor $\tilde{\boldsymbol{\varepsilon}}$ and the macroscopic strain tensor $\boldsymbol{\varepsilon}$ is given as

$$\tilde{\boldsymbol{\varepsilon}} = \boldsymbol{\beta}^{\mathrm{T}} : \boldsymbol{\varepsilon}. \tag{40}$$

By substituting (38) and (40) into (39) we can write

$$\boldsymbol{\sigma} = \boldsymbol{\beta} : \tilde{\boldsymbol{\sigma}} = \boldsymbol{\beta} : \boldsymbol{C}^{\mathrm{e}} : \tilde{\boldsymbol{\varepsilon}} = \boldsymbol{\beta} : \boldsymbol{C}^{\mathrm{e}} : \boldsymbol{\beta}^{\mathrm{T}} : \boldsymbol{\varepsilon}, \tag{41}$$

therefore the secant stiffness tensor is obtained as

$$\boldsymbol{C} = \boldsymbol{\beta} : \boldsymbol{C}^{\mathrm{e}} : \boldsymbol{\beta}^{\mathrm{T}}. \tag{42}$$

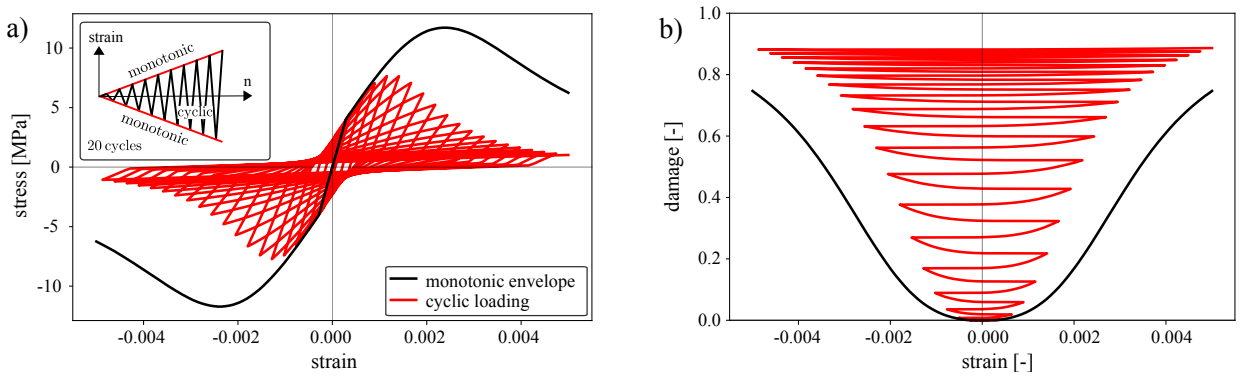

Figure 3: The tangential behavior at the microplane level (CSD): a) monotonic and cyclic stress-strain relationship; b) the corresponding damage evolution

The fourth order inverse damage tensor can be written as

$$\beta_{ijkl} = \frac{1}{4}(\phi_{ik}\delta_{jl}+\phi_{il}\delta_{jk}+\phi_{jk}\delta_{il}+\phi_{jl}\delta_{ik}), \quad (43)$$

In this modeling approach we assume that the tensile behavior is governed by the normal microplane damage, and the compressive behavior is governed by the plastic normal behavior and the cumulative sliding damage.

The second order integrity tensor $\boldsymbol{\phi}$ and the elastic stiffness tensor in the evaluation of the instantaneous material stiffness (42) are given as

$$\begin{aligned}\phi_{ij} &= \frac{3}{2\pi}\int_\Omega \phi^{\text{mic}}\, n_i n_j d\Omega \qquad (44)\\ &= \frac{3}{2\pi}\int_\Omega \sqrt{(1-\omega^{\text{mic}}(n))}\, n_i n_j d\Omega,\end{aligned}$$

$$\boldsymbol{C}^{\text{e}}_{ijkl} = \lambda\delta_{ij}\delta_{ij} + \mu(\delta_{ik}\delta_{jl}+\delta_{il}\delta_{jk}). \quad (45)$$

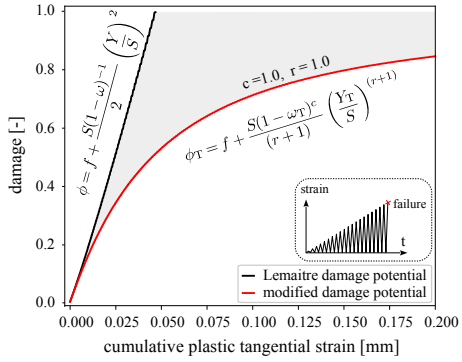

Figure 4: Comparison between the Lemaitre damage potential and the modified potential: damage evolution vs. cumulative sliding/plastic strain under cyclic increased loading scenario

Plastic strain tensor: According to [14] the macroscopic plastic strain tensor can be obtained by integrating microplane plastic strains as follows

$$\begin{aligned}\varepsilon^{p}_{ij} &= \frac{3}{2\pi}\int_\Omega \varepsilon_N^{p,\text{mic}} n_i n_j d\Omega\\ &+ \frac{3}{2\pi}\int_\Omega \frac{\varepsilon_{Tr}^{\pi,\text{mic}}}{2}(n_i\delta_{rj}+n_j\delta_{ri})d\Omega. \qquad (46)\end{aligned}$$

Macroscopic stress tensor: The macroscopic stress tensor can be obtained as follows

$$\boldsymbol{\sigma} = \boldsymbol{\beta} : \boldsymbol{C}^{\text{e}} : \boldsymbol{\beta}^{\text{T}} : (\boldsymbol{\varepsilon} - \boldsymbol{\varepsilon}^{\text{p}}). \quad (47)$$

Macroscopic dissipated energy: The macroscopic energy dissipation can be obtained as

$$\mathcal{D}^{\text{mac}} = \frac{3}{2\pi}\int_\Omega (\mathcal{D}_{\text{N}}^{\text{mic}} + \mathcal{D}_{\text{T}}^{\text{mic}})\, d\Omega \quad (48)$$

3 ELEMENTARY STUDIES

To study and evaluate the model behavior under elementary loading conditions simulations at the level of a single material point are now presented. As emphasized in [10], single material point simulations are important to verify the fundamental model behavior and to calibrate the model parameters. A benchmark test data for different concrete types from the literature are used to evaluate the model response. For this analysis, the numerical integration over the hemisphere has been performed with $n_{\text{mp}} = 28$ number of microplanes.

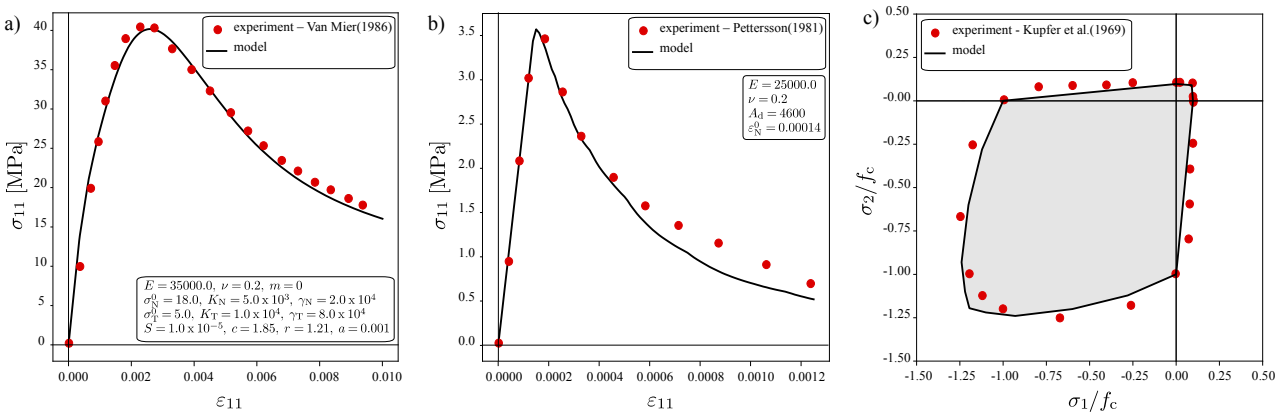

Figure 5: Elementary study of the model behavior under monotonic loading with comparison to experimental results: a) uniaxial compression ; b) uniaxial tension; c) biaxial failure envelope

Fig. 5a, shows the simulation with parameters adjusted to fit the uniaxial compression test data presented by [15]. Another simulation shown in Fig. 5b presents the fit for uniaxial tension test data presented by [16]. The test data reported in [17], leading to the biaxial failure envelope depicted in Fig. 5c, is compared with the numerical results obtained using the model.

To elucidate the internal structure of the introduced model, an elementary example of the model behavior exposed to uniaxial compressive fatigue strain loading is depicted in Fig. 6. In the example, the parameters obtained from the uniaxial compression test shown in Fig. 5a have been used. The stress-strain relationship for the monotonic and fatigue loading with three different strain ranges up to 100 cycles is shown in Fig. 6a. The corresponding compressive stress decrease at maximum strain over cycles "fatigue relaxation curve" for the different cases is presented in Fig. 6b. It shows a rapid decay of the compressive stress for the increased loading range. These curves document that the model can capture the degradation of the material during the cycling. This aspect is essential for fatigue modeling showing the degradation of the material strength under cyclic loading. Moreover, the model provides the possibility to separately quantify the fractions of energy dissipation associated with the introduced inelastic mechanisms.

The total and decomposed accumulated energy dissipation over cycles for the different strain ranges corresponding equations (48), (22) and (37) are depicted in Figs. 6c, d, e, respectively. The total macroscopic energy dissipation obtained as a summation of the energy dissipation owing to plastic strains, damage and the isotropic and kinematic hardening is plotted in Figs. 6c. The dissipated energy due to plastic strains and damage normal to a microplane are plotted in Figs. 6d, e respectively. For the parameters obtained from the uniaxial compression test Fig. 5a the total energy dissipation is dominated by the plasticity which shows a rapid accumulation of the dissipated energy in the first few cycles. The energy dissipation owing to damage mechanism shows a similar rapid accumulation of the dissipation energy to the plasticity with further quasi-linear accumulation after the first few cycles. The microplane sliding damage evolution at each microplane for the different four loading ranges is depicted in Figs. 6f, g, h showing that for the largest loading range plotted in the blue color, the sliding damage has propagated in a larger number of microplanes in comparison to the other loading ranges. The detailed evaluation of the energy dissipation is performed with the intention to establish an energetic treatment of the fatigue behavior in the future.

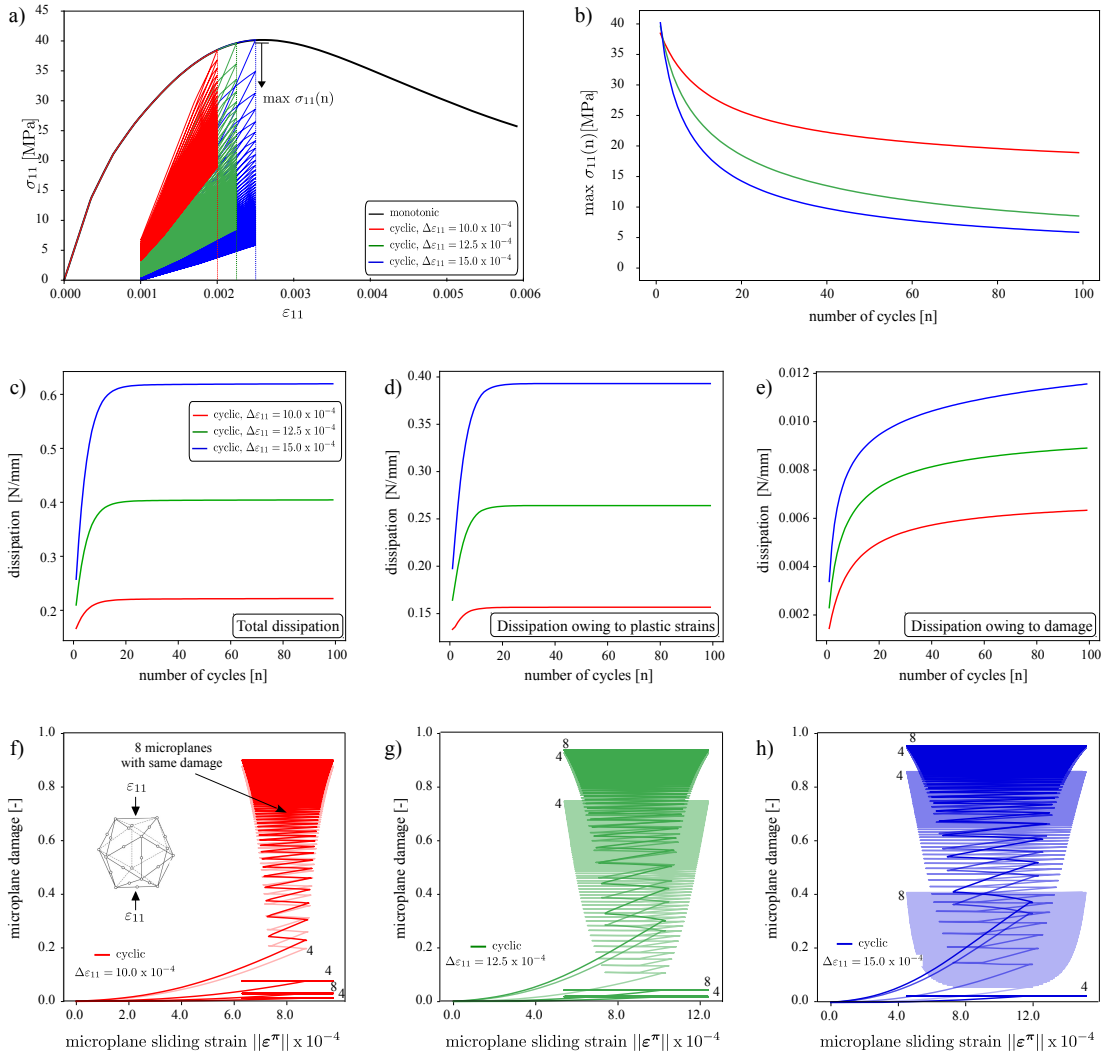

Figure 6: Example of the model behavior under compressive fatigue loading - strain controlled: a) stress-strain relationship; b) decrease of the compressive stress with the number of cycles; c) total energy dissipation; d) energy dissipation owing to plastic strains; e) energy dissipation owing to damage; f, g, h) sliding damage at the different microplanes for the different loading ranges

4 HYSTERETIC LOOPS

An assumption for the accurate evaluation of energy dissipation is an ability to capture the shape of the hysteretic loops. In this section the proposed microplane fatigue model is compared with two selected tensorial modeling approaches from the literature [4, 6] for concrete fatigue under compression as representatives of different fatigue damage hypotheses.

The first modeling approach presented by Alliche [4] with the fatigue damage linked to the total strains uses the framework for viscoplasticity modeling and replaces the traditional yield limit by an irreversibility condition to reflect the effect of the loading-unloading on damage at sobritical load levels. The model is based on the fatigue damage hypothesis proposed by Marigo [3] postulating that the damage evolves only during the loading process described as follows

$$\dot{\omega} = \begin{cases} \text{loading stage } (\dot{\omega} > 0) \\ \text{unloading stage } (\dot{\omega} = 0) \end{cases} \tag{49}$$

The second modeling approach proposed by Desmorat *et al.* [6] relates the fatigue damage to a cumulative sliding strains. In particular, the

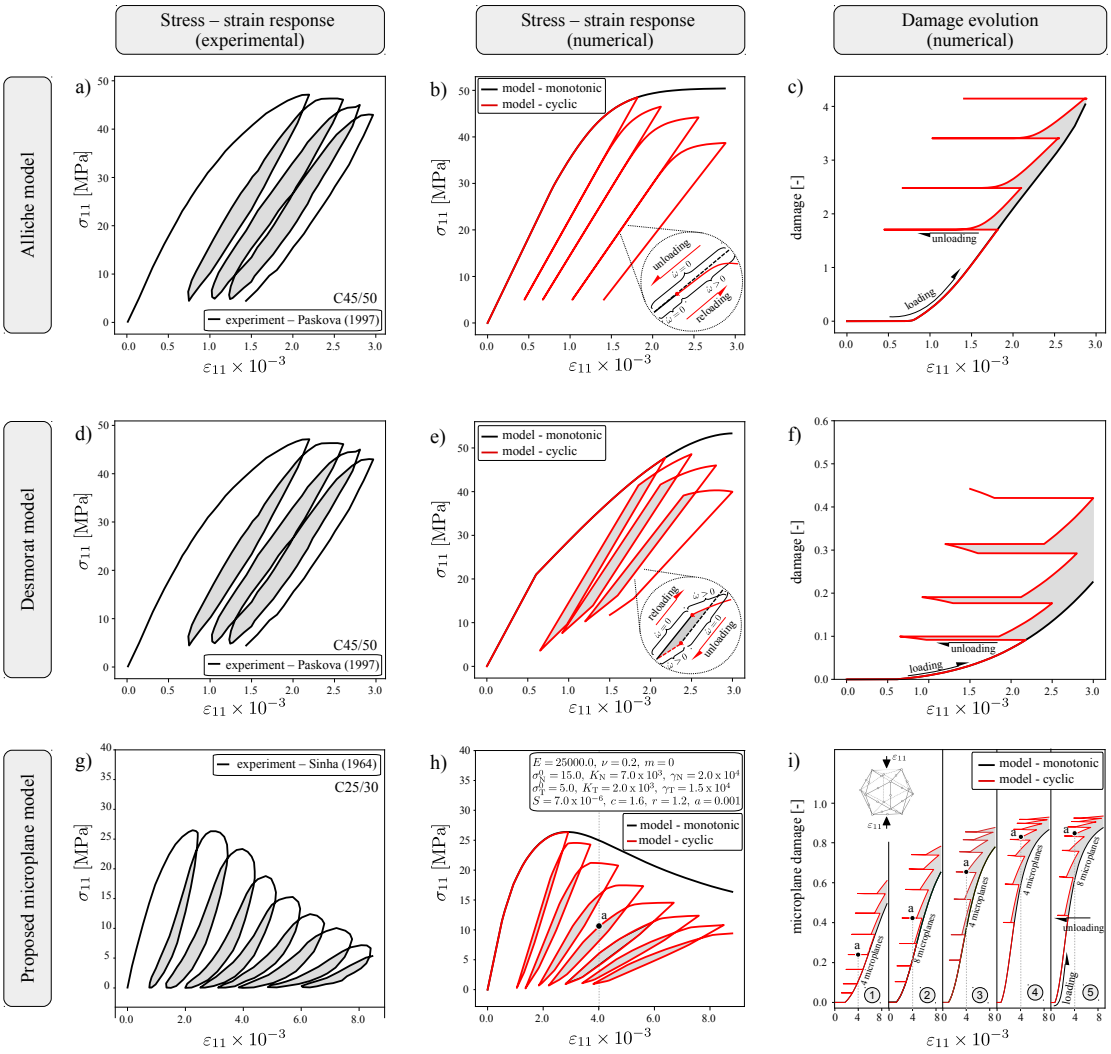

Figure 7: Comparison study in terms of hysteretic loops between existing macro-scale fatigue models (Alliche model, Desmorat model) and the proposed microplane model

fatigue damage hypothesis introduced in [7] is used to link the damage rate with the absolute value of the inelastic strain rate as follows

$$\dot{\omega} = f\left(|\dot{\varepsilon}^{\pi}|\right) \tag{50}$$

The hysteretic loops represent the history dependence of the stress-strain relationship upon loading and reloading. To evaluate the ability of the modeling approaches to represent the typical shape of hysteretic loops, a comparison study is presented in Fig. 7.

An example of a stress-strain response under uniaxial compression showing the experimental results for concrete 45/50 reported in [18] is displayed in Fig. 7a. The simulated response using the Alliche model plotted in Fig. 7b. The calculated stress strain relationship reveals that unloading and reloading follows identical paths. The obvious reason for this is due to the assumption that the fatigue damage is directly linked to the total strain, without explicitly distinguishing the evolution of plastic strain during the loading and reloading steps. The zoomed view to the lower load level shows the decreasing stiffness visualizing the principle idea of the Marigo fatigue damage hypothesis [3]. The damage evolution in correspondence to the cyclic stress loading is plotted in Fig. 7c.

In Desmorat model introducing the elastic-plastic split and the fatigue damage hypothesis proposed by Lemaitre [7], the damage evolution is linked to the plastic/sliding strain. As a con-

sequence, the opening of the hysteretic loops can be reproduced as documented in Fig. 7e. Interestingly enough, the performed study documents that the fatigue damage does not grow only at the upper load level but may also increase in the lower loading level. The damage evolution corresponding to the cyclic stress loading is plotted in Fig. 7f.

The cyclic uniaxial compression test data presented by [19] is depicted in Fig. 7g and compared with results obtained by the proposed microplane model in Fig. 7h together with the calculated monotonic envelope. The shape of the obtained hysteretic loops during the cyclic loading history shows an acceptable agreement with the experimental results. The numerical results show progressive degradation of the compressive stress during the cyclic loading and also a smoother shape of the the hysteretic loops in comparison with the results obtained by Desmorat model. The damage is evolving over the individual cycles gradually and can reproduce the experimentally observed shape of the hysteretic loop in a better way than the considered tensorial macro-scale models.

To illustrate the aspect of damage homogenization the damage state in a material point is visualized in a resolved form showing the damage at the relevant microplanes in Fig. 7i. The state (a) at the fourth loading cycle pointed with black circle in Fig. 7h shows that the stress-strain exhibits some nonlinearity upon the reloading stage. The corresponding microplane damage state depicted in Fig. 7i for five groups of microplanes with equal damage state due to symmetry reveals that the nonlinearity of the stress-strain response at the state (a) is due to the evolution of the damage at the microplanes of the groups (4) and (5) in Fig. 7i.

This particular observation documents the ability of the model to capture the stress redistribution in a material point due to anisotropic evolution of damage. As emphasized in [8] this feature is a paramount requirement for a reproduction of damage evolution at subcritical load levels.

5 CONCLUSIONS

The proposed microplane model is formulated within the thermodynamic framework enabling a flexible integration of dissipative mechanisms at the level of a microplane. The key idea of the proposed model is to relate the fatigue damage to a cumulative inelastic sliding strain introduced in the tangential plane at the microplane level.

Initial studies using the proposed model show a plausible reproduction of the test data on concrete compression under cyclic loading available in the literature. The cumulative sliding damage introduced at the microplane level as a source of fatigue damage presents a promising possibility to consistently describe the fatigue behavior of concrete under compression loading. At the same time, microplane theory with an inherent homogenization concept integrating the response of all microplanes within the tensorial macroscopic representation provides an explicit evaluation of dissipated energy and its rate. Further systematic calibration and validation procedures of the model with regularization technique will be conducted in the future.

Acknowledgment

The work was supported by *the Deutsche Forschungsgemeinschaft* (DFG) (Project No. 412131890). This support is gratefully acknowledged.

REFERENCES

[1] F. Liu, J. Zhou, Fatigue strain and damage analysis of concrete in rein-forced concrete beams under constant amplitude fatigue loading, Shock and Vibration 2016. doi:10.1155/2016/3950140.

[2] D. Pfanner, Zur degradation von stahlbetonbauteilen unter ermüdungsbeanspruchung. konstruktiven ingenieurbau. Ruhr-universiät bochum (2003).

[3] J. Marigo, Modelling of brittle and fatigue damage for elastic material by growth

of microvoids,Engineering Fracture Mechanics,21(4)(1985) 861-874.

[4] A. Alliche, Damage model for fatigue loading of concrete, International Journal of Fatigue,26(9)(2004) 915-921.

[5] V. M. Kindrachuk, M. Thiele, J. F. Unger, Constitutive modeling of creep-fatigue interaction for normal strength concrete under compression, International Journal of Fatigue,78(2015)81-94.

[6] R. Desmorat, F. Ragueneau, H. Pham, Continuum damage mechanics for hysteresis and fatigue of quasi-brittle materials and structures, International Journal for Numerical and Analytical Methods in Geomechanics 31(2)(2007)307-329.

[7] J. Lemaitre, R. Desmorat, Engineering damage mechanics: ductile,creep, fatigue and brittle failures, Springer Science and Business Media,2005.

[8] K. Kirane, Z. P. Bažant, Microplane damage model for fatigue of quasibrittle materials: Sub-critical crack growth, lifetime and residual strength, International Journal of Fatigue 70 (2015)93-105.

[9] Y. Wang, Physical stochastic damage model for concrete subjected to fatigue loading, International Journal of Fatigue 121 (2019) 191 196. doi.org/10.1016/j.ijfatigue.2018.12.023.

[10] Caner, F.C., Bažant, Z.P., 2013b. Microplane Model M7 for Plain Concrete. II: Calibration and Verification. Journal of Engineering Mechanics 139,1724-1735.

[11] Jirasek, M., 1999. Comments on Microplane Theory, in: Mechanics of Quasibrittle Materials and Structures.Hermes Science Publications, pp. 55-77.

[12] F. Ragueneau, N. Dominguez, A. Ibrahimbegovic, Thermodynamic-based interface model for cohesive brittle materials: Application to bond slip in RC structures, Computer Methods in Applied Mechanics and Engineering 195 (52)(2006) 7249-7263.

[13] Baktheer, Abedulgader, and Rostislav Chudoba. "Pressure-sensitive bond fatigue model with damage evolution driven by cumulative slip: Thermodynamic formulation and applications to steel-and FRP-concrete bond." International Journal of Fatigue 113 (2018): 277-289. doi.org/10.1016/j.ijfatigue.2018.04.020

[14] Ignacio Carol and Zdeněk P. Bažant. Damage and plasticity in microplane theory. In:International Journal of Solids and Structures34.29 (1997), pp 3807-3835.

[15] Van Mier and Jan G. M., Multiaxial strain-softening of concrete, Materials and Structures (1986),19-3, PP 1871-6873, issn:1871-6873.

[16] Petersson, Per-Erik, Crack growth and development of fracture zones in plain concrete and similar materials (1981), Division, Inst.

[17] Kupfer, Helmut and Hilsdorf, Hubert K and Rusch, Hubert, Behavior of concrete under biaxial stresses, Journal Proceedings (1969),66-8, PP 656-666.

[18] T. Paskova, C. Meyer, Low-cycle fatigue of plain and fiber-reinforcedconcrete, Materials Journal 94 (4) (1997) 273286. doi:10.14359/309.

[19] Sinha, BP and Gerstle, Kurt H and Tulin, Leonard G, Hubert K and Rusch, Hubert, Stress-strain relations for concrete under cyclic loading, Journal Proceedings (1964),61-2, PP 195-212.